JOURNAL OF MATERIALS SCIENCE 30 (1995) 4861–4870

Mechanical properties of extruded dual-phase NiAl Alloys

R. TIWARI, S. N. TEWARI
Chemical Engineering Department, Cleveland State University, Cleveland, OH 44 115, USA
R. ASTHANA, A. GARG
NASA Lewis Research Center, Cleveland, OH 44 135, USA

The mechanical behaviour of dual-phase microstructures, consisting of elongated primary NiAl grains aligned with an intergranular NiAl/*X* eutectic phase, produced by extrusion of cast NiAl-*X* (where *X*=Cr and W) alloys, has been examined. Chromium, added to create a dual-phase NiAl-based aligned microstructure, resulted in large increases in the yield strength, but only marginal improvement in the toughness. In contrast, tungsten alloying leads to ductility or toughness increases with no significant strengthening. The constitutional hardening rate due to deviations from stoichiometry in Ni rich NiAl was estimated to be about 66 MPa (Ni^{-1} at%).

1. Introduction

The ordered intermetallic NiAl(β) has emerged as a suitable candidate material for gas turbine engine components because of its high melting point, low density, good oxidation resistance, high thermal conductivity, high temperature thermodynamic stability and high stiffness. However, the lack of room temperature ductility and toughness is its major shortcoming [1, 2]. The lack of room temperature ductility has been attributed to the presence of insufficient independent slip systems (only three), which inhibits plastic deformation in polycrystalline NiAl. Several concepts have been explored to improve its room temperature tensile ductility. These include attempts to alter the slip behaviour (activate ⟨1 1 1⟩ slip) by microalloying [3], martensitic phase transformation toughening [4], microalloying of single crystal NiAl [5] and ductile phase toughening [6].

The first evidence of ductile phase toughening of NiAl was provided in the directionally solidified Ni–34 Fe–9.9 Cr–18.2 Al (at %) alloy, whose microstructure consisted of alternating lamellae of nickel rich face centred cubic (fcc) solid solution, γ phase, and β phase (about 40 vol % β) [7]. This *in situ* composite material exhibited almost 17% tensile elongation at room temperature with fracture occurring by cleavage of the β-NiAl phase which was sandwiched between ductile necked regions of γ. Recently, a Ni–30 Al alloy has been directionally solidified to produce aligned rod like γ′ (fcc intermetallic phase Ni_3Al) in a β-NiAl matrix (about 40 vol % β phase) with 10% room temperature ductility [6]. Another alloy, Ni–30 Fe–20 Al, when directionally solidified, contained aligned β-NiAl and γ/γ′ phases, and showed 10% ductility [6]. Heat treatment of extruded Ni–30Al–20 Co and Ni–36 Al was used to produce a microstructure of equiaxed β-NiAl grains containing a necklace of continuous γ′ at the grain boundary [8]. The microstructure with the γ′ necklace exhibited a slight improvement (about 0.5%) over almost zero ductility of those without the γ′. Ishida et al. [9] forged and rolled several alloys (Ni–20 Cr–20 Al, Ni–25 Al–18 Fe, Ni–15 Al–65 Fe and Ni–26 Al–50 Co) to obtain microstructures containing uniform distribution of equiaxed β and γ grains, which showed room temperature ductilities varying from 2 to 6%. Extrusion of cast Ni–20 Al–30 Fe alloy has been carried out to produce a microstructure of fine equiaxed β distributed in β + γ′ eutectic [10]. The alloy showed 8–22% room temperature ductility depending upon the fineness of the γ′ grains. It has been suggested [6, 11] that the ductility enhancement is brought about because of

1. the inhibition of crack nucleation in the β phase due to the increased mobile dislocation density, and
2. the inhibition of crack propagation by plastic stretching of the ductile phase in the crack (crack bridging).

However, all these alloys, utilizing ductile phase toughening concepts, contain large amounts of alloying elements. This would affect adversely the useful properties of NiAl, its high melting point and its low density. In addition, large amounts of certain alloying elements tend to degrade its outstanding oxidation resistance (significant deviation from stoichiometry is known to degrade the oxidation resistance of NiAl, which is contingent upon the formation of a stable Al_2O_3 layer).

The purpose of this exploratory research was to produce a dual-phase microstructure with the least amount of alloy additives and explore its room and elevated-temperature mechanical properties. Examination of the NiAl based pseudobinary eutectic phase diagrams, NiAl–Cr [12, 13], NiAl–Mo [14, 15] and NiAl–W [15, 16], suggested that extrusion of cast

0022–2461

microstructures consisting of the proeutectic β grains surrounded by a small amount of intergranular eutectic, while avoiding recrystallization during or immediately after the extrusion, may result in a microstructure consisting of β grains aligned with the extrusion direction and the intergranular regions occupied with Cr, Mo or W phases. The solid solubility of Cr and W in β-NiAl is less than that of Mo in the temperature regime of NiAl extrusion, 1300–1450 K. The NiAl–Cr and NiAl–W alloys were selected for this investigation, because the amount of solute addition to β-NiAl, required to yield a stable two–phase microstructure at the extrusion temperatures, would be less as compared with NiAl-Mo.

2. Experimental procedure

The NiAl, NiAl–W and NiAl–Cr alloys were induction melted and chill cast under a protective argon atmosphere in a high purity copper mould to obtain cylindrical castings (14 cm long and 5 cm diameter). Differential thermal analysis (DTA) was carried out on the alloy castings to determine the phase transformation temperatures, and select an optimum extrusion temperature. The castings were vacuum encapsulated in steel cans and extruded at 1400 K to an extrusion ratio of 32:1 for NiAl and NiAl–W, and 16:1 for NiAl–Cr. The chemical compositions of the alloys were determined by inductively coupled emission spectroscopy techniques. The microstructures were examined, following metallographic preparation and etching with saturated molybdic acid, by optical microscopy.

The as-extruded bars were centreless ground and machined for compressive (cylinders: length, 1.25 cm; diameter, 0.63 cm), tensile (buttonhead specimens: gauge diameter, 0.3 cm; gauge length, 3.0 cm), and four-point bend notched fracture toughness (length, 2.54 cm; cross-section, 0.25 × 0.25 cm; notch, 0.13 cm deep and 0.25 cm wide) tests. Compression tests were performed in air at a strain rate of 1.74×10^{-4} s^{-1} in the temperature range 300–1000 K. The tensile specimens were electropolished prior to testing. The tensile tests were carried out in air at a strain rate of 1.3×10^{-4} s^{-1} at 300 and 800 K. Fracture toughness was determined at room temperature by four-point bend testing of the notched bar specimens with the loading direction normal to the extrusion axis. For the compression specimens, the cracks originating at the specimen surface and propagating into the specimen interior were examined by scanning electron microscopy (SEM). These specimens were then cut normal to the compression axis and polished to examine the crack paths by optical metallography. The fracture surfaces after tensile and four-point bend tests were examined by SEM.

Microstructures of the NiAl, NiAl–Cr and NiAl–W alloys were also examined using a transmission electron microscope (TEM) operating at 120 kV. Compression test specimens, loaded to the yield point, were sectioned by electric discharge machining to obtain 3 mm diameter discs. The TEM specimens were obtained by electrochemical polishing these discs in a twin-jet polisher using a solution of 70% ethanol, 14% distilled water, 10% butyl cellosolve and 6% perchloric acid, cooled to 263 K. An applied potential of 20–50 V, with a corresponding current of 10–15 mA, produced the electron transparent foils.

3. Results

The chemical composition of the NiAl, NiAl–W and NiAl–Cr alloys, obtained by induction plasma techniques, were Ni–46 Al, Ni–48.3 Al–1 W and Ni–43 Al–9.7 Cr (at %), respectively. The carbon and oxygen contents of these alloys were determined to be lower than 0.012 wt%. The alloy densities were, 5.45 ± 0.10 for NiAl, 5.93 ± 0.09 for Ni–48.3 Al–1 W and 5.57 ± 0.05 for Ni–43 Al–9.7 Cr (g cm^{-3}).

3.1. Microstructural characterization

3.1.1. Ni–43 Al–9.7Cr

Fig. 1a shows the NiAl-Cr pseudobinary eutectic phase diagram. Fig. 1b shows the DTA results obtained from the Ni–43 Al–9.7 Cr alloy examined in this study. The solvus, solidus and liquidus temperatures indicated by the peaks marked V, T and D in Fig. 1b are 1478, 1720 and 1818 K, respectively. These are in reasonable agreement with the phase transformation temperatures estimated from the phase diagram for the 9.7 at % Cr alloy (the composition

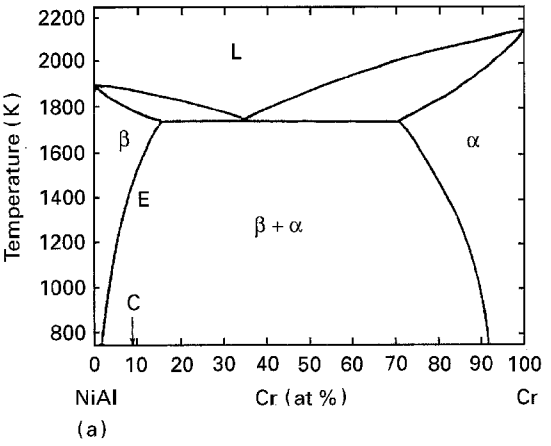

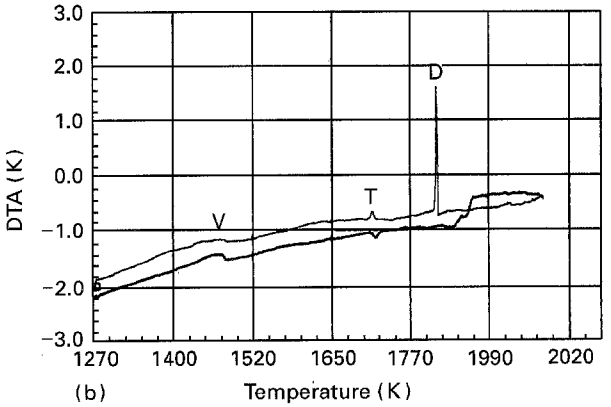

Figure 1 (a) The NiAl-rich portion of the pseudobinary NiAl–Cr eutectic phase diagram [10], with composition C, of the Ni–43 Al–9.7 Cr alloy used in this study; (b) typical DTA plot obtained for the Ni–43 Al–9.7 Cr alloy used in this study.

marked by the arrow, C, in Fig. 1a). The temperature of extrusion, 1398 K, indicated by point E in Fig. 1a lies in the β + Cr two-phase field.

The microstructures of the cast and extruded Ni–43 Al–9.7 Cr alloy are shown in Fig. 2. The as-cast Ni–43 Al–9.7 Cr alloy consisted of β-NiAl dendrites and the interdendritic NiAl–Cr eutectic (Fig. 2a). As expected, the extrusion of the Ni–43 Al–9.7 Cr alloy in a two-phase regime resulted in the formation of a two-phase microstructure consisting of β-NiAl grains, aligned with the extrusion axis, and a fine intergranular NiAl-Cr eutectic microconstituent. This is evident from the transverse (normal to the extrusion axis) and longitudinal microstructures presented in Fig. 2b, c, respectively. The β-NiAl grain size measured on the transverse sections (perpendicular to the extrusion direction), Fig. 2b, was about 15 μm. This is much smaller than the grains in the as-cast alloy, about 30 μm (Fig. 2a). The equiaxed β-NiAl grains, typically observed in extruded NiAl (Fig. 3a), are not observed in the extruded Ni–43 AlAl–9.7 Cr alloy.

3.1.2. Ni–46 Al and Ni–48.3 Al–1 W

The extruded Ni–46 Al showed an equiaxed grain morphology with relatively fine grain size (25–50 μm), due to recrystallization during and subsequent to extrusion, Fig. 3a. The longitudinal microstructure of

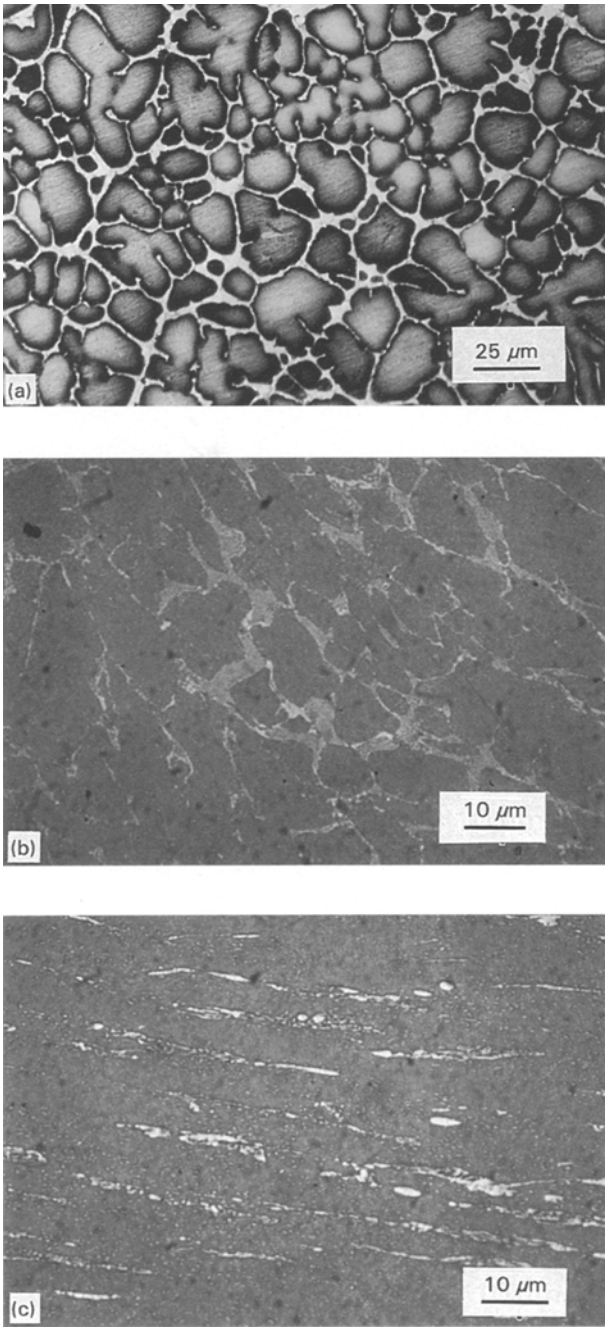

Figure 2 Microstructures of (a) as-cast, (b) transverse (normal to the extrusion direction) and (c) longitudinal views of the extruded Ni–43 Al–9.7 Cr alloy. The NiAl–Cr eutectic phase is present as stringers surrounding the aligned NiAl grains.

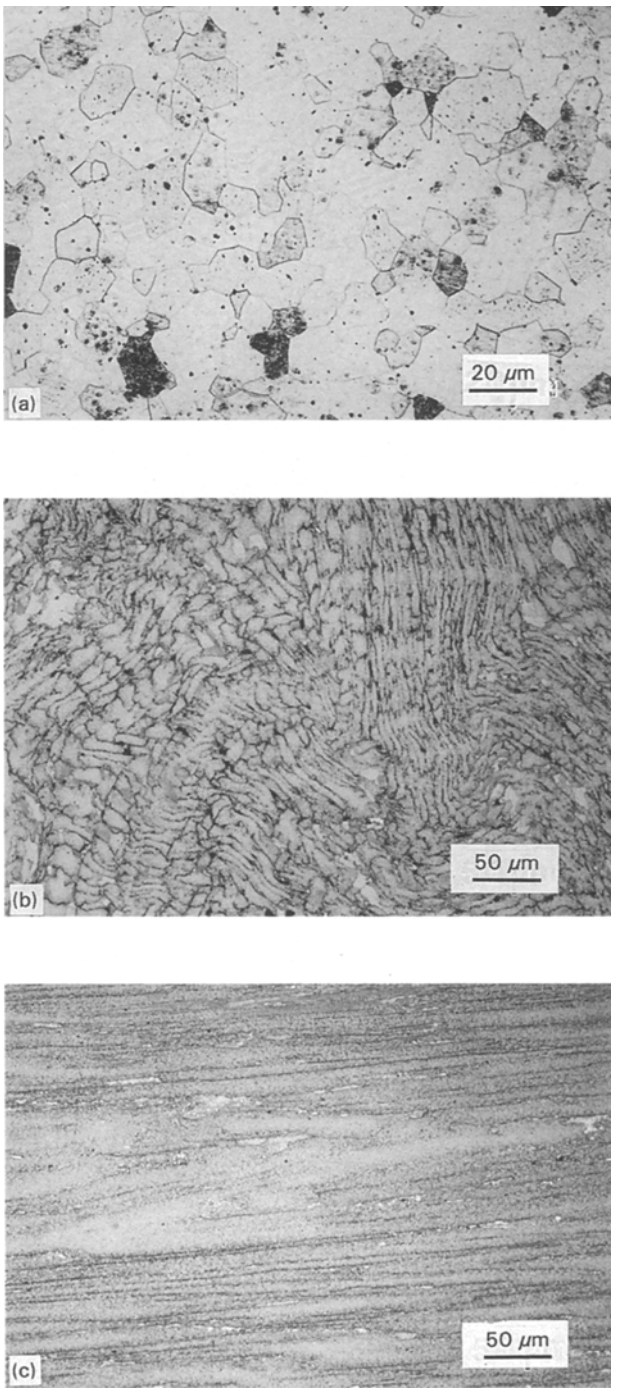

Figure 3 Microstructures of (a) extruded NiAl in transverse section showing the equiaxed grain structure, (b) transverse and (c) longitudinal sectional views of the extruded Ni–48.3 Al–1 W alloy (the NiAl–W eutectic phase is present as stringers surrounding the NiAl grains).

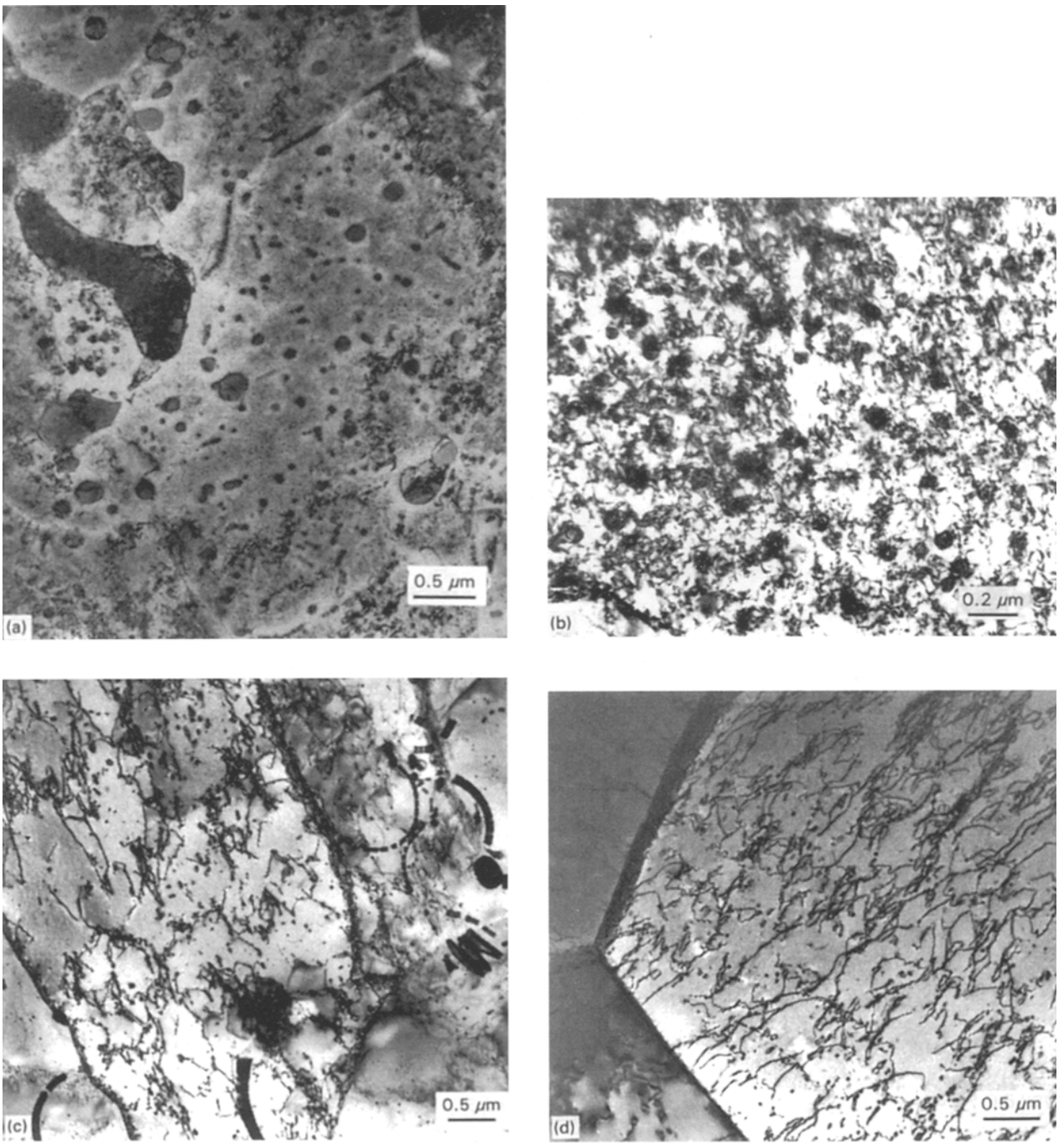

Figure 4 Transmission electron micrographs of (a) Ni–43 Al–9.7 Cr, (b) Ni–43 Al–9.7 Cr alloy showing dislocation pinning by the α-chromium precipitates, (c) Ni–48.3 Al–1 W and (d) Ni–46 Al.

extruded NiAl, on sections parallel to the extrusion direction (not shown here), also had a similar equiaxed grain appearance.

The transverse and longitudinal microstructures of the extruded Ni–48.3 Al–1 W alloy are shown in Fig. 3b, c. Extrusion of this alloy also led to the formation of a two-phase aligned microstructure, which consisted of β-NiAl grains surrounded by the NiAl–W eutectic. The β-NiAl grains in Ni–48.3 Al–1 W alloy are considerably smaller in size, 5–20 μm (Fig. 3b), than in the NiAl alloy.

3.1.3. TEM examination

Transmission electron micrographs of the Ni–43 Al–9.7 Cr, Ni–48.3 Al–1 W, and Ni–46 Al alloy specimens, deformed just beyond the compressive yield stress, are shown in Fig. 4a–d. The Ni–43 Al–9.7 Cr matrix contains a bimodal distribution of α-chromium precipitates, about 15 nm in size, spaced at 50 nm, and about 45 nm in size, spaced at 150 nm (Fig. 4a). Occasionally, $Cr_{23}C_6$ precipates, not shown in Fig. 4a, were also observed. Extensive dislocation pinning associated with the 45 nm chromium precipitates is evident from Fig. 4b. The tungsten-containing alloy has approximately 50 nm tungsten precipitates spaced at about 135 nm (Fig. 4c). The dislocation density in this alloy is much smaller than in the chromium containing alloy. Both tungsten and chromium alloyed NiAl specimens showed subgrain formation. This was not observed in Ni–46 Al (Fig. 4d). The Ni–46 Al sample showed the least amount of dislocations.

3.2. Compressive deformation and fracture

Typical engineering stress–strain curves for the compressive deformation at 300 K are shown in Fig. 5a for the extruded Ni–46 Al, Ni–43 Al–9.7 Cr and Ni–48.3 Al–1 W alloys. Sudden stress (or load) drops are observed in the Ni–46 Al. The Ni–48.3 Al–1 W and Ni–43 Al–9.7 Cr alloys did not show these load drops, and the load displacement curves were smooth. The load drops were not observed in the extruded Ni–46 Al at 800 K, where the load–displacement curves were smooth.

Temperature dependence of the 0.2% offset compressive yield strength (CYS) for the extruded Ni–46 Al, Ni–43 Al–9.7 Cr and Ni–48.3 Al–1 W alloys is shown in Fig. 5b. Three tests were performed at room temperature to examine the experimental reproducibility. At other temperatures, only one test was performed for all the alloys.

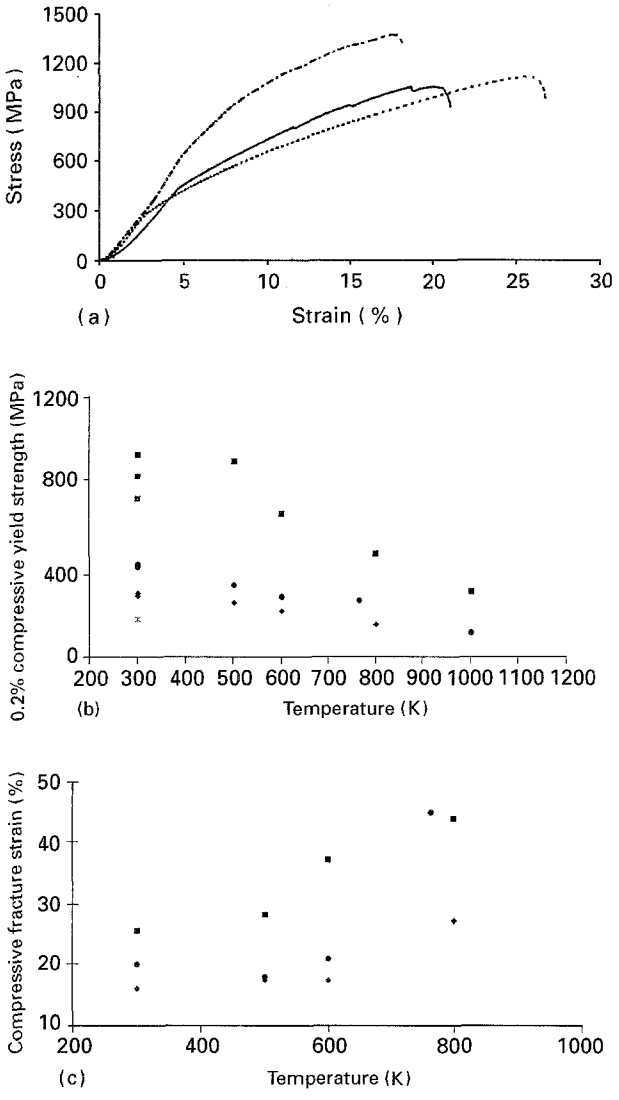

Figure 5 (a) Typical stress–strain curves, at 300 K, for the three alloys examined in this study (-●-)Ni–43 Al–9.7 Cr, (——) Ni–46 Al, (– – –) Ni–48.3 Al–1 W; (b) Variation of 0.2% compressive yield strength (CYS) with temperature for the extruded (●) Ni–46 Al, (■) Ni–43 Al–9.7 Cr and (◆) Ni–48.3 Al–1 W alloys, (*) data of Cotton *et al.* [3] for Ni–50 Al; (c) Variation of compressive fracture strain (defined in the text), obtained during compression testing of the extruded (●) Ni–46 Al, (■) Ni–48.3 Al–1 W and (◆) Ni–43 Al–9.7 Cr alloys.

The room temperature compressive yield strength of the extruded Ni–43 Al–9.7 Cr alloy (895 ± 90 MPa) is nearly twice that of the extruded Ni–46 Al (451 ± 6 MPa). It is also larger than the room temperature CYS of extruded Ni–45 Al–5 Cr alloy, 818 ± 9 MPa [3]. The room temperature CYS of the extruded Ni–48.3 Al–1 W alloy (311 ± 5 MPa) is, however, lower than that of the extruded Ni–46 Al (451 ± 6 MPa). The room temperature CYS of extruded Ni–50 Al, 189 ± 6 MPa [3] is significantly lower than that of the alloys examined in this study.

The Ni–43 Al–9.7 Cr shows the highest CYS throughout the temperature range 300–1000 K for all the alloys examined in this study. It is more than twice that of the other two alloys. The temperature dependence of the Ni–46 Al and Ni–48.3 Al–1 W alloys is similar, showing a continuous decrease with increasing temperature. The temperature dependence of the Ni–43 Al–9.7 Cr is different. Its CYS remains constant up to about 500 K before it begins to decrease. The extruded Ni-46 Al retains its strength advantage over Ni–48.3 Al–1 W up to about 800 K. At 1000 K both the alloys show similar strengths.

The compressive fracture strains, defined as the total strain when a drastic drop in the compressive stress due to the specimen fracture occurs during compression testing, are shown in Fig. 5c for the three alloys. At 300 K, the Ni–48.3 Al–1 W alloy has a higher compressive fracture strain compared to Ni–46 Al, while the Ni–43 Al 9.7 Cr has a lower compressive fracture strain compared to the Ni–46 Al alloy. Specimens were observed to fracture until 600 K for Ni–48.3 Al–1 W, 800 K for Ni–46 Al and 1000 K for Ni–43 Al–9.7 Cr. At temperatures higher than these, due to the excessive specimen plasticity, the compression testing had to be interrupted in order to prevent damage to the test equipment. This suggests that the brittle–ductile transition temperatures (BDTT) for the three alloys might be in the following order: Ni–48.3 Al–1 W < Ni–46 Al < Ni–43 Al–9.7 Cr.

Figs 6–8 present the room temperature compressive fracture behaviour of the three alloys. The fracture in Ni–46 Al appears to be mixed-mode, with predominance of transgranular fracture (Fig. 6). The Ni–43 Al–9.7 Cr alloy shows a predominantly transgranular fracture, with the crack propagation being mostly through the primary β-NiAl grains (Fig. 7a). However, some evidence of crack path following the intergranular eutectic boundaries is also present (Fig. 7a). Its fracture surface gives a dimpled appearance (Fig. 7b) as opposed to the predominantly sharp-faceted appearance in the extruded Ni–46 Al (Fig. 6b), due to the grain boundary decohesion. The dimpled appearance is presumably caused by the pull-out of the intergranular chromium phase. This indicates some toughening potential of the Ni–43 Al–9.7 Cr alloy.

The extruded Ni–48.3 Al–1 W alloy also fractures in the intergranular mode at room temperature, with the cracks propagating along the grain boundaries (Fig. 8a). However, the fracture surface for the extruded Ni–48.3 Al–1 W alloy gives a dimpled appearance (Fig. 8b) as opposed to the predominantly sharp facets of the grain boundaries in extruded Ni–46 Al

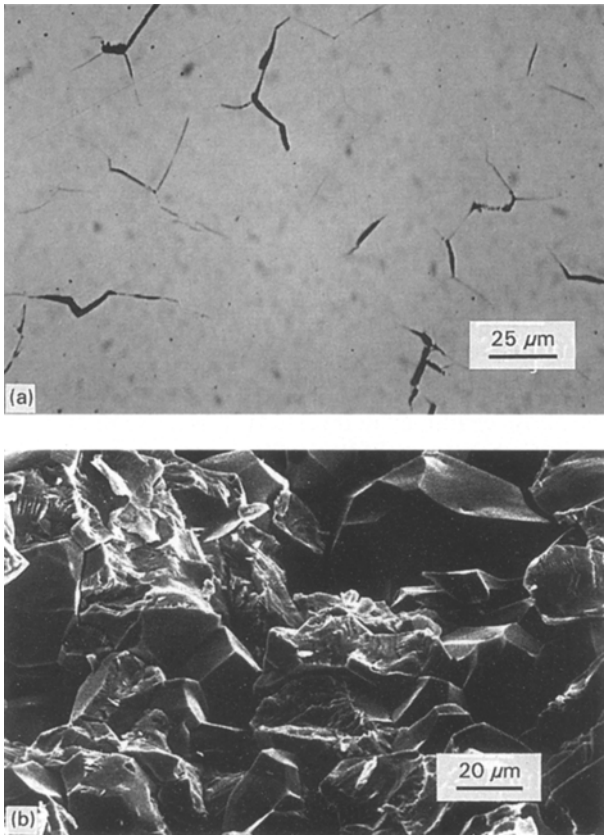

Figure 6 Microstructure showing crack path, and (b) fracture surface of extruded Ni–46 Al, compression tested at 300 K, showing intergranular failure.

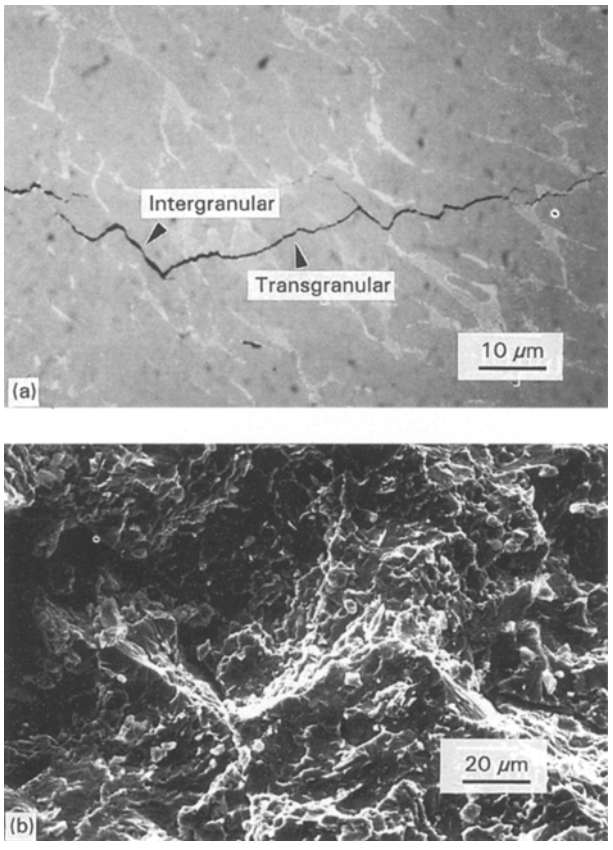

Figure 7 Microstructure showing crack path, and (b) fracture surface of extruded Ni–43 Al–9.7 Cr alloy, compression tested at 300 K, showing mixed mode (trans and intergranular) fracture.

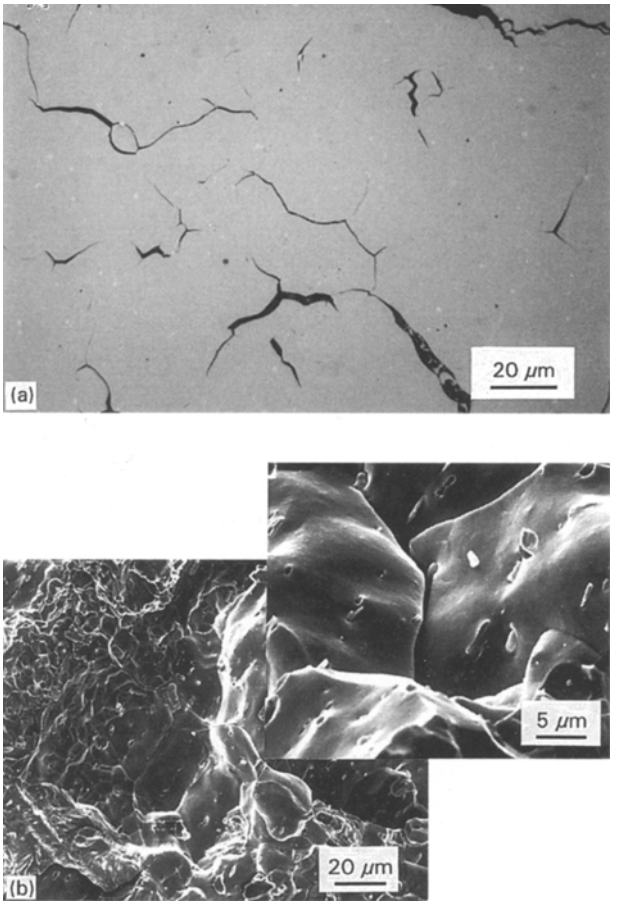

Figure 8 Microstructure showing crack path, and (b) fracture surface of extruded Ni–48.3 Al–1 W alloy, compression tested at 300 K, showing intergranular failure.

(Fig. 6b). This is conceivably because of the tungsten precipitates either getting pulled out or in some cases getting plastically stretched. This behaviour is more evident in the inset of Fig. 8b, and may lead to improved room temperature fracture toughness.

At 800 K, both Ni–46 Al (Fig. 9a) and Ni–43 Al–9.7 Cr (Fig. 9b) alloys, showed transgranular fracture. Regions of inhomogeneous deformation (deformation bands) were observed in NiAl. These were not observed for Ni–43 Al–9.7 Cr. The nature of crack propagation in Ni–48.3 Al–1W alloy could not be determined because it was very ductile at 800 K and showed no radial surface cracks. For the extruded Ni–43 Al–9.7 Cr alloy, although the 800 K fracture is transgranular, the interdendritic NiAl–Cr eutectic appears to cause some crack deflection (indicated by arrows in Fig. 9b).

3.3. Tensile deformation and fracture

The tensile properties of the extruded NiAl, Ni–48.3 Al–1 W and Ni–43 Al–9.7 Cr alloys, at 300 K, are summarized in Table I. The table also includes data for the cast and extruded Ni–50 Al reported by Cotton *et al.* [3]. The Ni–46 Al showed brittle behaviour (no yielding or plastic deformation), with a tendency for the specimens to fail in the grip, near the end of the gauge section. The yield strength value has, therefore, been indicated as greater than the maximum

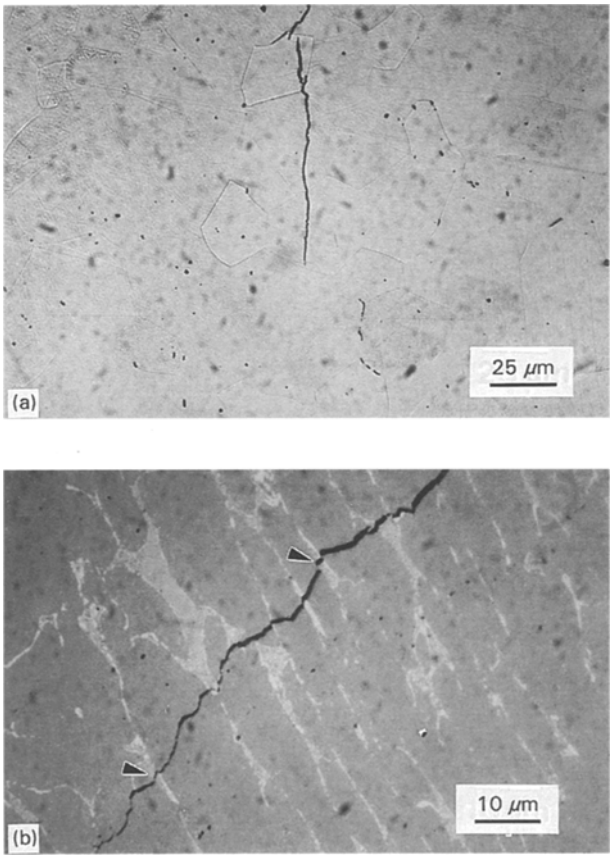

Figure 9 Microstructures showing transgranular crack propagation in extruded (a) Ni–46 Al and (b) Ni–43 Al–9.7 Cr, compression tested at 800 K.

observed stress. This value is greater than 180 MPa, reported for Ni–50 Al [3]. The plastic strain for the Ni-50 Al is reported to be 1.5% [3] as compared with the zero ductility of the present Ni–46 Al alloy. This is in agreement with the observation [17] that Ni-rich off-stoichiometry leads to an increased strength and decreased ductility for the alloys. This observation is also valid at higher temperatures. For example, the Ni–50 Al alloy has a yield strength of 100 MPa and ductility of 70% at 600 K [3], as compared with 253 MPa yield strength and 6.3% ductility for the Ni–46 Al alloy at 800 K.

The Ni–48.3 Al–1 W alloy showed distinct yielding, its 0.2% offset yield strength being 205 $\pm$ 20 MPa and plastic strain 1.2%. It is interesting to note that the room temperature yield strength of the Ni–48.3 Al–1W is smaller than that of Ni–46 Al ($>$ 279 MPa). One would expect that tungsten alloying would lead to strengthening due to solid solution hardening (tungsten dissolved in β-NiAl) and precipitation hardening (fine tungsten precipitates in β-NiAl). However, apparently the Ni–Al ratio has a more pronounced influence on the yield strength than these effects. Possible synergism between non-stoichiometry and solid solution strengthening must also be considered. The room temperature yield strength of the Ni–48.3 Al–1 W alloy is almost identical to that of the Ni-48.9 Al alloy (220 MPa) [18], suggesting that tungsten alloying (up to 1%) has virtually no influence on the yield strength of NiAl. However, tungsten alloying does improve room temperature ductility, as indicated by 1.2% for Ni–48.3 Al–1 W versus nearly zero for Ni–49 Al [19].

Similar to room temperature behaviour, at 800 K the yield strength of Ni–48.3 Al–1 W(150 MPa) is smaller than that of Ni–46 Al (253 MPa). However, the ductility of Ni–48.3 Al–1 W (30.2%) is much larger than that of Ni–46 Al (6.3%).

The Ni–43 Al–9.7 Cr alloy showed the highest yield strength of all the alloys examined in this study, both at room temperature and at 800 K. Its ductility was zero at room temperature, and 3% at 800 K. The 800 K ductility data (Table I) suggest that the BDTT of these alloys are in the following order, Ni–43 Al–9.7 Cr > Ni–46 Al > Ni–48.3 Al–1 W. This is in agreement with the previously described compressive fracture behaviour of these alloys. The BDTT of NiAl alloys increases with increased deviation from stoichiometry [20, 21]. The nickel–aluminium ratio for the Ni–43 Al–9.7 Cr, Ni–46 Al and Ni–48.3 Al–1 W alloys are, respectively, 1.17, 1.10 and 1.05. One would therefore expect Ni–46 Al to have a higher BDTT than Ni–43 Al–9.7 Cr. This is contrary to the observed behaviour, and may be attributed to the chromium alloying, which is known to increase the BDTT of NiAl alloys [3].

The fracture surfaces of the room temperature tensile tested Ni–46 Al, Ni–43 Al–9.7 Cr and Ni–48.3 Al–1 W are shown in Fig. 10. The fracture behaviour of Ni–46 Al (Fig. 10a) appears to be predominantly transgranular, with occasional intergranular failure. This is in agreement with earlier observation of transgranular failure in Ni–45 Al by Nagpal and Baker [22]. The grain boundaries, however, appear to provide some resistance to crack growth as evidenced by the sharp facets observed along the grain boundaries on the fracture surface. For the Ni–43 Al–9.7 Cr alloy, the fracture is transgranular (Fig. 10b). The fracture surface shows that the chromium precipitates, located within the matrix and at the β–NiAl grain boundaries, get pulled out during crack growth. This should result in improved fracture toughness. In the Ni–48.3 Al–1 W alloy, necking and subsequent fracture (or pull-out) of the ductile tungsten phase located on the grain boundaries is seen (Fig. 10c). The pulled-out tungsten phase appears to leave behind cavities (inset of Fig. 10c) although matching-surface fractography is needed to confirm this.

3.4. Fracture toughness

The room temperature fracture toughness values, K_c, of the Ni–46 Al, Ni–43 Al–9.7 Cr and Ni–48.3 Al–1 W are given in Table I. These represent the average of three measurements on each of the alloys. The room temperature fracture toughness of Ni–46 Al was 4.9 MPa $m^{1/2}$, in agreement with the values reported for polycrystalline NiAl, 4–6 MPa $m^{1/2}$ [4]. The Ni–43 Al–9.7 Cr alloy, with a K_c value of 5.4 MPa $m^{1/2}$, showed a 10% increase in fracture toughness. The Ni–48.3 Al–1 W showed the largest K_c, 5.9 MPa $m^{1/2}$, about 22% higher than for Ni–46 Al. The

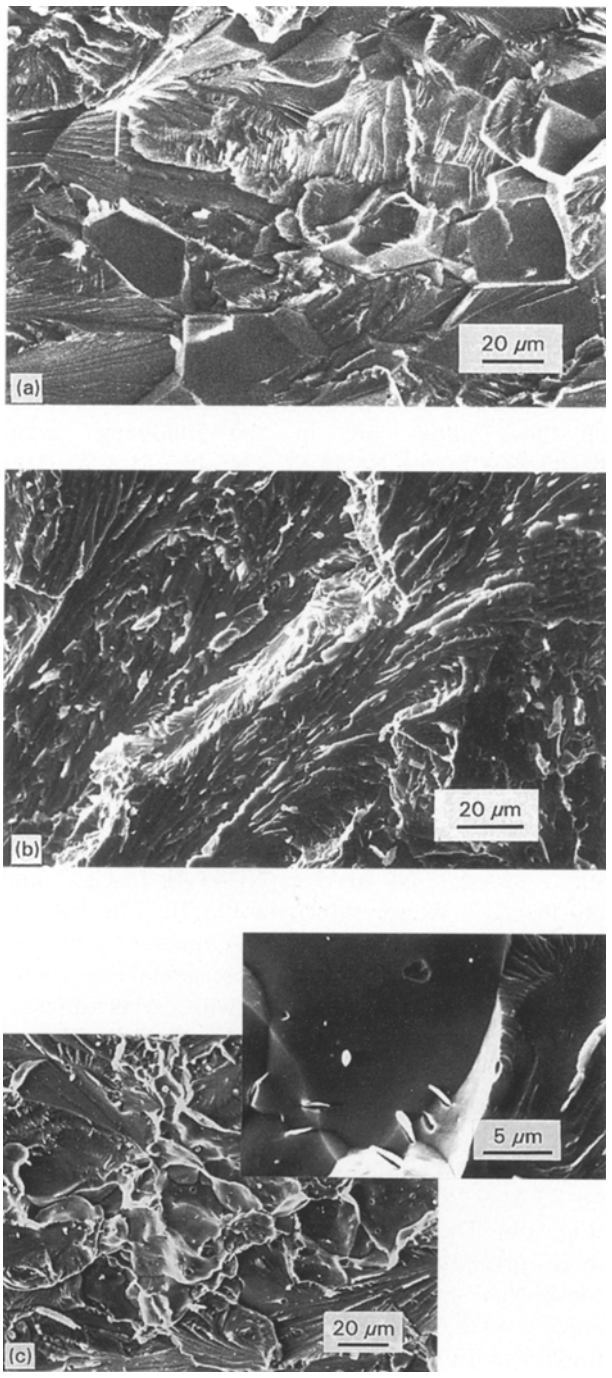

Figure 10 Fracture surfaces of room temperature tensile tested (a) Ni–46 Al, (b) Ni–43 Al–9.7 Cr, and (c) Ni–48.3 Al–1 W alloys.

fracture for all these alloys was transgranular, and showed the characteristics described above for the room temperature tensile fracture, i.e. pulled out chromium and tungsten particles for the Ni–43 Al–9.7 Cr and Ni–48.3 Al–1 W alloys.

4. Discussion

4.1. Microstructure

Primary dendrites of NiAl nucleate first and grow during casting of the hypoeutectic NiAl–X (where X = Cr and W) alloys. The low solid state diffusivities of solutes leads to an increase in the solute content of the remaining melt, which eventually reaches the eutectic composition, C_E, (for NiAl–Cr: $C_E = 33$ at % Cr) and solidifies as the interdendritic eutectic, as seen in Fig. 2a. Since the extrusion temperatures, the NiAl phase is considerably weaker than chromium (yield strength of Ni–50 Al < 43 MPa [3] at 800 K; whereas the yield strength for Cr equals 98 MPa at 1073 [23], and W equals 59 MPa at 1920 K [24]), the presence of the intergranular eutectic phase permits deformation only along the extrusion axis and yields the aligned microstructure (Fig. 2c). A microstructure with small grain size of the primary NiAl phase (which can be controlled by the rate of heat extraction during casting) is ideally suited for such extrusion processing in the two-phase regime.

4.2. Mechanical properties

It is well documented [18], and also observed in this study, that a deviation from stoichiometry, either by the formation of nickel vacancies (aluminium-rich alloys), or the substitutional nickel atoms on the aluminium sites (nickel-rich alloys), leads to NiAl strengthening. The room temperature compressive yield strength of the Ni–46 Al alloy (451 ± 6 MPa) is greater than that of Ni–50 Al (189 MPa) [3]. Assuming a linear dependence this increase in strength corresponds to a strengthening rate of 66 MPa (at % Ni^{-1}) for the Ni-rich NiAl compositions. This hardening rate agrees well with that deduced by Noebe et al. [2], 70 MPa (at % Ni^{-1}), from the tensile strength values of the Ni-rich cast and extruded NiAl alloys [17].

TABLE I Tensile properties of Ni–46 Al, Ni–50 Al [3], Ni–48.3 Al–1 W and Ni–43 Al–9.7 Cr alloy at 300 and 800 K

Alloy	0.2% offset compressive yield strength (MPa)	0.2% offset yield strength (MPa)	Ultimate tensile strength (MPa)	Fracture strain (%)	K_c (MPa $m^{1/2}$)
At 300 K					
Ni–46 Al	451	> 279	–	0.00	4.9
Ni–48.3 Al–1 W	312	205 ± 20	360	1.20	5.9
Ni–43 Al–9.7 Cr	895	> 496	–	0.00	5.4
Ni–50 Al [3]	189	180	–	1.50	–
Ni–50 Al–0.28 Fe [28]	210	160	185	–	
At 800 K					
Ni–46 Al	228	253	352	6.30	–
Ni–48.3 Al–1 W	167	150	205	30.20	–
Ni–43 Al–9.7 Cr	518	446	583	2.95	–

TABLE II Estimation of yield strengths of the Ni–45 Al–5Cr and Ni–43 Al–9.7 Cr alloys

Strengthening mechanism	Ni–45 Al–5 Cr (MPa)	Ni–43 Al–9.7 Cr (MPa)
Binary Ni–50 Al [3]	189	189
Solid solution strengthening [25]	431	431
Constitutional strengthening	174	157
Precipitation strengthening [25]	53	159
Estimated yield strength	847	937
Experimental yield strength	818 [3]	895

A microstructure, as observed in the extruded Ni–43 Al–9.7 Cr alloy, is expected to derive its strength from the following factors

1. Constitutional strengthening due to the variation in the Ni–Al ratio [66 MPa (at pct Ni^{-1}), as determined in this study].

2. Solid solution strengthening from the chromium dissolved in the NiAl phase. Cotton *et al.* [25] have reported a solid solution hardening rate of 287 MPa (at % Cr^{-1}).

3. Precipitation strengthening (chromium precipitates in the NiAl phase): the strength increment due to the obstruction of dislocation motion by non-shearing particles (dislocation pinning seen in Fig. 4b) can be estimated, in a manner similar to Cotton *et al.* [3], by the following expression

$$\Delta\sigma_p = \frac{Gb}{2\pi(\lambda - d)} \ln\left(\frac{d}{b}\right)$$

where G is the shear modulus (72 GPa), b the Burger's vector (0.2886 nm), d the Cr precipitate size (45 nm) and λ the interparticle spacing (150 nm). The strengthening contribution from the finest chromium precipitates has been ignored because dislocation pinning associated with these precipitates was not observed (Fig. 4b). These precipitates were apparently sheared because of the coherent interface between NiAl and Cr.

4. Grain size strengthening: earlier studies indicate that the yield strength of stoichiometric Ni–50 Al is dependent on the grain size and that this dependence increases with the deviation from stoichiometry [25, 26]. However, in Ni–43 Al–9.7 Cr alloy, the grain size of the primary β-NiAl phase, 15 μm, is considerably larger than the interparticle spacing between the Cr precipitates (150 nm). The mean free path for the dislocations will, therefore, be considerably less than the grain size. Hence, the grain size strengthening may be neglected in estimating the yield strength.

Table II compares the theoretical and experimentally measured compressive yield strengths of the Ni-43 Al–9.7 Cr and Ni–45 Al–5 Cr [3] alloys. The theoretical yield strength values have been computed by adding constitutional hardening [66 MPa (at % Ni^{-1}) for Ni-rich NiAl], solid solution hardening [287 MPa (at % Cr^{-1})] [25] and precipitation hardening, to the yield strength of binary Ni–50 Al (189 MPa) [3]. Since the Ni–45 Al–5 Cr alloy showed recrystallized β-NiAl grains having no interdendritic β-NiAl-Cr eutectic [3], all of the chromium in the alloy is assumed to be available for the solid solution and precipitation hardening of the matrix. As can be seen in Table II, the difference between the experimental and theoretical (estimated) yield strength values, for both the Ni–45 Al–5 Cr and Ni–43 Al–9.7 Cr alloys, is less than 5%.

An examination of Table I shows that for the three alloys examined in this study the compressive yield strength values are greater than the tensile yield strengths. For example for the Ni–48.3 Al–1 W the compressive yield strength at room temperature is about 108 MPa larger than the tensile yield strength. No such information can be deducted for the Ni–46 Al and Ni–43 Al–9.7 Cr at room temperature because they failed prior to yielding. However, as indicated in Table I, similar behaviour has been observed in the cast plus extruded Ni–50 Al [27] and Ni Al–0.2 at % Fe [28] alloys at room temperature. This difference decreases with increasing temperature, e.g. from 108 MPa at 300 K to 17 MPa at 800 K for the Ni–48.3 Al–1 W. Similar behaviour is seen for the Ni–50 Al alloy extruded from the vacuum atomized powder, their compressive strengths being higher than the tensile strengths by 70 and 20 MPa at 500 and 900 K, respectively [27]. While this difference at 800 K for the Ni–46 Al and Ni–48.3 Al–1 W alloys is insignificant, it is considerably larger (72 MPa) for the Ni–43 Al–9.7 Cr alloy.

4.3. Toughening Mechanism

The primary cause of the improved fracture toughness in extruded Ni–48.3 Al–1 W appears to be the crack bridging by the presence of a ductile tungsten phase. Since the brittle chromium phase in the Ni–43 Al–9.7 Cr alloy is not plastically deformed, it does not yield significant toughening. The minimal toughening obtained in this alloy as compared to the extruded Ni–46 Al is due to the pull-out of the chromium phase. Increased tungsten alloying would be more effective in increasing the room temperature fracture toughness of the extruded NiAl alloys, as compared to the increased chromium alloying.

5. Conclusions

The following conclusions may be drawn from this study on the mechanical behaviour of dual-phase aligned microstructures produced by casting and extrusion of the hypoeutectic NiAl–X (where X = Cr or W) alloys

1. Extrusion of dual phase microstructure prevents the dynamic recrystallization that is commonly observed in single phase NiAl.

2. The compressive yield strengths for all the extruded alloys are larger than the tensile yield strengths. Their difference decreases with increasing temperature.

3. Chromium alloying leads to a two-fold increase in the yield strength of NiAl, presumably due to solid solution strengthening and precipitation strengthening.

4. Tungsten addition is more effective in ductility and/or toughness improvement of NiAl, as compared to chromium.

Acknowledgements

This research was partially supported by a grant from the NASA Lewis Research Center. Appreciation is expressed to Dr. J. D. Whittenberger for providing the extruded material, and to R. R. Toothman, R. E. Phillips and W. Karpinski for assistance with the mechanical testing. Continuous encouragement by T. K. Glasgow is gratefully acknowledged.

References

1. D. B. MIRACLE, *Acta. Metall. Mater*, **41** (1993) 649.
2. R. D. NOEBE, R. R. BOWMAN and M.V. NATHAL, *Int. Met. Rev.* **38** (1993) 193.
3. J. D. COTTON, R. D. NOEBE and M. J. KAUFMAN, *Intermetallics* **1** (1993) 3.
4. K. S. KUMAR, S. K. MANNAN and R. K. VISWANADHAM, *Acta Metall. Mater.* **40** (1992) 1201.
5. R. DAROLIA, D. LAHRMAN and R. FIELD, *Scripta Metall. Mater.* **126** (1992) 1007.
6. R. D. NOEBE, A. MISRA and R. GIBALA, *ISIJ Int.* **31** (1991) 1172.
7. S. N. TEWARI, NASA TN D-8355 (NASA, Lewis Research Center, Cleveland, OH, 1977).
8. D. R. PANK, M. V. NATHAL and D. A. KOSS, *J. Mater. Res.* **5** (1990) 942.
9. K. ISHIDA, R. KAINUMA, N. UENO and T. NISHIZAWA, *Metall. Trans. A* **22A** (1991) 441.
10. S. GUHA, P.R. MUNROE and I. BAKER, *Mater. Res. Symp. Proc.* **133** (1989) 633.
11. R. GIBALA, H. CHANG, C. M. CZARNIK, K. M. EDWARDS and A. MISRA, in "Structural Intermetallics", edited by R. Darolia, J. J. Lewandowski, C. T. Liu, P. L. Martin, D. B. Miracle and M. V. Nathal (The Minerals and Metals Society, 1993) pp. 561–567.
12. J. D. COTTON, R. D. NOEBE and M. J. KAUFMAN, *Phase Equilibria* submitted.
13. S. M. MERCHANT and M. R. NOTIS, *Mater. Sci. Engng* **66** (1984) 47.
14. S. B. MASLENKOV and V. A. RODMKINA, *Izvestiya Akademii Nauk SSSR, Metally* **1** (1989) 194.
15. P. NASH, S. FIELDING and D. R. F. WEST, *Met. Sci.* **17** (1983) 192.
16. L. KAUFMAN and H. NESOR, *Can Metall. Quart.* **14** (1975) 221.
17. K. H. HAHN and K. VEDULA, *Scripta Metall. Mater.* **23** (1989) 7.
18. R. T. PASCOE and C. W. A. NEWEY, *Met. Sci. J.* **2** (1968) 138.
19. E. M. SCHULSON, *Mater. Res. Soc. Symp. Proc.* **39** (1985) 193.
20. J. H. WESTBROOK, H. E. GRENOBLE and D. L. WOOD, WADD-TR-60-184, Pt V, (1964) p. 22.
21. C.C. LAW and M. J. BLACKBURN, Final Technical Report No. AFWAL-TR-87-4102, (1987).
22. P. NAGPAL and I. BAKER, *Mater. Character.* **27** (1991) 167.
23. "Metals Handbook", desk edition (ASM International, 1985).
24. "High Temperature Materials II", edited by G. M. Ault, W. F. Barclay and H. P. Munger (Wiley, New York, 1963).
25. J. D. COTTON, R. D. NOEBE and M. J. KAUFMAN, "Structural Intermetallics", edited by R. Darolia, J. J. Lewandowski, C. T. Liu, P. L. Martin, D. B. Miracle and M. V. Nathal (The Minerals and Metals Society, 1993) pp. 513–522.
26. I. BAKER, P. NAGPAL, F. LIU and P. R. MUNROE, *Acta. Metall. Mater* **39** (1991) 1637.
27. R. R. BOWMAN, R. D. NOEBE, S. V. RAJ and I. E. LOCCI, *Met. Trans A* **23A** (1992) 1493.
28. K. MATSUGI, D. W. WENMAN and N. S. STOLOFF, *Scripter Met.* **27** (1992) 1633.

Received 4 October 1994
and accepted 11 April 1995